



Water Formation in Non-Hydrolytic Sol–Gel Routes: Selective Synthesis of Tetragonal and Monoclinic Mesoporous Zirconia as a Case Study

Yanhui Wang, Maroua Bouchneb, Rimeh Mighri, Johan G Alauzun, P. Hubert Mutin

► To cite this version:

Yanhui Wang, Maroua Bouchneb, Rimeh Mighri, Johan G Alauzun, P. Hubert Mutin. Water Formation in Non-Hydrolytic Sol–Gel Routes: Selective Synthesis of Tetragonal and Monoclinic Mesoporous Zirconia as a Case Study. *Chemistry - A European Journal*, 2021, 27, pp.2670-2682. 10.1002/chem.202003081 . hal-03032788

HAL Id: hal-03032788

<https://hal.science/hal-03032788>

Submitted on 1 Dec 2020

HAL is a multi-disciplinary open access archive for the deposit and dissemination of scientific research documents, whether they are published or not. The documents may come from teaching and research institutions in France or abroad, or from public or private research centers.

L'archive ouverte pluridisciplinaire **HAL**, est destinée au dépôt et à la diffusion de documents scientifiques de niveau recherche, publiés ou non, émanant des établissements d'enseignement et de recherche français ou étrangers, des laboratoires publics ou privés.

Materials Science | Hot Paper

 Water Formation in Non-Hydrolytic Sol–Gel Routes: Selective Synthesis of Tetragonal and Monoclinic Mesoporous Zirconia as a Case StudyYanhui Wang, Maroua Bouchneb, Rimeh Mighri, Johan G. Alauzun, and P. Hubert Mutin*^[a]

Abstract: Several non-hydrolytic sol–gel syntheses involving different precursors, oxygen donors, and conditions have been screened aiming to selectively produce mesoporous t-ZrO₂ or m-ZrO₂ with significant specific surface areas. The *in situ* water formation was systematically investigated by Karl Fisher titration of the syneresis liquids. XRD and nitrogen physisorption were employed to characterize the structure and texture of the ZrO₂ samples. Significant amounts of water were found in several cases, notably in the reactions of Zr(OnPr)₄ with ketones (acetone, 2-pentanone, acetophenone), and of ZrCl₄ with alcohols (benzyl alcohol, ethanol) or acetone. Conversely, the reactions of Zr(OnPr)₄ with acetic

anhydride or benzyl alcohol at moderate temperature (200 °C) and of ZrCl₄ with diisopropyl ether appear strictly non-hydrolytic. Although reaction time and reaction temperature were also important parameters, the presence of water played a crucial role on the structure of the final zirconia: t-ZrO₂ is favored in strictly non-hydrolytic routes, while m-ZrO₂ is favored in the presence of significant amounts of water. ¹H and ¹³C NMR analysis of the syneresis liquids allowed us to identify the main reactions responsible for the formation of water and of the oxide network. The morphology of the most interesting ZrO₂ samples was further investigated by electron microscopy (SEM, TEM).

Introduction

Mesoporous oxides are of primary importance in the areas of heterogeneous catalysis, adsorption, separation or energy. Non-hydrolytic sol–gel (NHSG) or non-aqueous sol–gel provides simple, cost-effective routes for the synthesis of non-ordered mesoporous metal oxides or mixed oxides, avoiding the use of reactivity modifiers, templates or supercritical drying.^[1,2] NHSG is performed in non-aqueous medium and the oxygen of the oxide network is not provided by added water but by organic compounds (e.g. ethers, alcohols, ketones, etc.).^[1,2] Importantly, NHSG involves organic reaction pathways, and the moderate reactivity of C–O bonds results in easily manageable reaction rates, facilitating the control of the structure and texture. Even if the starting reaction mixture is anhydrous, water may be produced *in situ* by organic reactions, such as alcohol dehydration, esterification, or aldol condensation. In addition, hydroxyl (M–OH) groups resulting from non-hydrolytic hydroxylation reactions^[3] can condense together with formation of

water. Accordingly, only a few routes involving only aprotic reactions are strictly non-hydrolytic or non-aqueous.^[3,7] The presence of water in the reaction medium can impact not only the mechanism of formation of the oxo bridges, but also the structure, surface chemistry, morphology or texture of the final nanomaterials.^[5,7,8] However, there have been very few attempts at quantifying the water in NHSG reactions, and studies comparing water formation in different NHSG routes for a given oxide are lacking.

In this work we investigated the formation of water and its influence on the structure of the final oxide for nine different NHSG routes, involving two precursors and seven O-donors. As a case study, we chose the synthesis of mesoporous ZrO₂.

Indeed, ZrO₂ is an important catalytic material owing to its high thermal stability, the presence of both acid and basic sites and its oxidizing and reducing properties.^[9–13] Moreover, the surface properties, activity and selectivity of zirconia-based catalysts depend on the structure of the ZrO₂ phase.^[12–16] At atmospheric pressure, three polymorphs are known for bulk ZrO₂: the monoclinic phase (m-ZrO₂) is stable up to 1170 °C, the tetragonal phase (t-ZrO₂) is stable between 1170 °C and 2370 °C, and the cubic phase (c-ZrO₂) above 2370 °C. However, the tetragonal and cubic phases can be stabilized at room temperature up to a critical crystallite size of about 30 nm because their surface energy is lower than that of the monoclinic phase.^[17] The presence of lattice strain,^[18] impurities^[19,20] or oxygen vacancies^[21] also stabilizes the tetragonal phase. Accordingly, the synthesis in aqueous medium by conventional sol–gel/precipitation methods of high-surface area zirconia with controlled phase has attracted much attention.^[10,15,22–24]

[a] Dr. Y. Wang, Dr. M. Bouchneb, R. Mighri, Dr. J. G. Alauzun, Dr. P. H. Mutin
Institut Charles Gerhardt Montpellier, UMR 5253
Université de Montpellier, Montpellier (France)
E-mail: hubert.mutin@univ-montp2.fr

 Supporting information and the ORCID identification number(s) for the author(s) of this article can be found under:
<https://doi.org/10.1002/chem.202003081>.

 © 2020 The Authors. Published by Wiley-VCH GmbH. This is an open access article under the terms of Creative Commons Attribution NonCommercial-NoDerivs License, which permits use and distribution in any medium, provided the original work is properly cited, the use is non-commercial and no modifications or adaptations are made.

Conversely, the synthesis of mesoporous ZrO_2 by NHSG routes remains practically unexplored. Jansen and Guenther obtained after calcination at 500 °C tetragonal zirconia by ester elimination between $\text{Zr}(\text{OAc})_4$ and $\text{Zr}(\text{OnPr})_4$,^[25] but the specific surface area was not reported. Warwar Damouny et al. reported that the reaction of ZrCl_4 with $i\text{Pr}_2\text{O}$ (ether route) led after calcination at 800 °C to a mixture of t- ZrO_2 and m- ZrO_2 phases with a low specific surface area ($16 \text{ m}^2 \text{ g}^{-1}$).^[26] On the other hand, the synthesis of ZrO_2 nanoparticles by two NHSG routes has been investigated. Although the particles were not calcined in order to avoid aggregation, crystalline particles were obtained owing to the high reaction temperatures used (200–340 °C). The alkoxide route involving the reaction of ZrCl_4 with $\text{Zr}(\text{O}i\text{Pr})_4$ - $i\text{PrOH}$ in the presence of a capping agent was used initially, leading to c- ZrO_2 or t- ZrO_2 particles.^[27,28] The most used route is the surfactant-free benzyl alcohol route, based on the reaction of zirconium alkoxides^[29–34] or zirconium chloride^[33,35] in benzyl alcohol at 200–270 °C in an autoclave. Due to the large number of parameters that influence the crystallinity (precursor, concentration, reaction temperature, time, liner material),^[31,32] the control of the structure by the benzyl alcohol route is not straightforward. Interestingly, two articles discuss the possible role of water. De Keukeleere et al. proposed that the formation of m- ZrO_2 nanoparticles in the reaction of benzyl alcohol with ZrCl_4 was due to the release of HCl, which catalyzed the formation of water by dehydration of benzyl alcohol. In the reaction of $\text{Zr}(\text{O}i\text{Pr})_4$ - $i\text{PrOH}$ with benzyl alcohol, they found that addition of water alone was not sufficient to promote the formation of m- ZrO_2 instead of c- ZrO_2 and that the addition of a strong acid was necessary.^[33] In a recent study Gambe et al. reported that water formed also in the reaction of $\text{Zr}(\text{O}i\text{Pr})_4$ - $i\text{PrOH}$ in benzyl alcohol, presumably by intramolecular dehydration of $i\text{PrOH}$, leading to tetragonal-monoclinic mixtures.^[34]

The aim of the present article is to thoroughly investigate the synthesis by different NHSG routes of mesoporous ZrO_2 supports, with controlled tetragonal or monoclinic structure, and to clarify the role of water, that is, to see if water is produced in other NHSG routes and if it governs the crystal structure.

In the first part of this work, several different non-hydrolytic routes and reaction conditions (temperature, time) were screened and the water content in the reaction medium was systematically measured by Karl Fisher titration. The texture and the crystalline structure of the different samples was investigated, aiming to identify conditions leading selectively to mesoporous t- ZrO_2 or m- ZrO_2 supports with significant specific surface area.

In the second part, the main parameters governing the final crystalline phase were identified and the major role of water was confirmed based on the data collected in the screening study.

In the third part, NMR analysis of the syneresis liquids was used to identify for the different NHSG routes the main reactions responsible for the formation of water and of the oxide network.

In the last part, the texture and morphology of selected ZrO_2 samples was investigated.

Results and Discussion

Part 1: Screening study

In order to find the conditions suitable for selectively obtaining after calcination mesoporous t- ZrO_2 or m- ZrO_2 and to establish the presence or absence of water in different NHSG routes, we synthesized a range of ZrO_2 samples by several non-hydrolytic sol-gel routes at various reaction temperatures and times, using two precursors, $\text{Zr}(\text{OnPr})_4$ (ZNP) and ZrCl_4 (ZCL), and seven O-donors, diisopropyl ether (DIPE), ethanol (EtOH), benzyl alcohol (BnOH), acetic anhydride (Ac_2O), acetophenone (AcPh), 2-pentanone (MPK) and acetone (ACE). In the non-hydrolytic sol-gel literature, O-donors such as ethers or acetic anhydride are used in a stoichiometric amount or in slight excess, while alcohols or ketones are usually used as both O-donor and solvent. In this work, we followed the same approach. For all of the syntheses, the amounts of precursor, O-donor and solvent (if any), the reaction temperature and reaction time are summarized in Table 1. In the following, the oxide samples (after calcination) are named after the precursor, the O-donor, the reaction temperature, and the reaction time as shown in Table 1. For example the ZrO_2 sample ZNP-AcPh 200/12 was prepared from $\text{Zr}(\text{OnPr})_4$ precursor by the acetophenone route at 200 °C for 12 h. The xerogel samples (before calcination) are indicated by the suffix “-X”, as in ZNP-AcPh 200/12-X.

We chose $\text{Zr}(\text{OnPr})_4$ rather than $\text{Zr}(\text{O}i\text{Pr})_4$ because of its higher thermal stability: Inoue et al. reported that the solvothermal decomposition of $\text{Zr}(\text{O}i\text{Pr})_4$ at 265 °C for 2 h gave amorphous zirconia whereas no reaction was observed at 300 °C with $\text{Zr}(\text{OnPr})_4$.^[56] $\text{Zr}(\text{OnPr})_4$ is commercially available as a 70 wt % solution in 1-propanol ($n\text{PrOH}$). However, $n\text{PrOH}$ is a potential O-donor and it can react with itself or other alcohols (dehydration), with Ac_2O (esterification), or with ketones (ketalization). To avoid such secondary reactions, $n\text{PrOH}$ was removed before use by treatment for 15 h under primary vacuum at 120 °C (Figure S1, Supporting Information).

To investigate the possible role of water, we used Karl Fischer titration to systematically quantify the water present in the liquid phase after reaction. The structure and texture of both the xerogels (non-calcined dried gels) and the final ZrO_2 samples were characterized by powder X-ray diffraction and nitrogen physisorption. The results are summarized in Table 2, and XRD patterns of selected samples are reported in Figures 1 and 2.

Formation of water during the reaction

Depending on the NHSG route and the reaction conditions, the water content in the syneresis liquids ranged from less than 10 ppm to nearly 20 000 ppm (i.e. 2 wt %). In addition, separation of an aqueous phase was observed for the last 3 samples of Table 2 (note that in these cases nearly all the acetone or benzyl alcohol was consumed during the reactions, as shown in Part 3). Actually, among all the reactions tested, only a few can be considered as strictly non-hydrolytic or non-

Table 1. Reaction conditions for the synthesis of zirconia samples from $\text{Zr}(\text{OnPr})_4$ and ZrCl_4 precursors.

Sample name	Precursor	O-donor	Solvent	Conditions
ZNP-Ac ₂ O 200/12	$\text{Zr}(\text{OnPr})_4$	Acetic anhydride	Toluene, 10 mL	200 °C, 12 h
ZNP-Ac ₂ O 200/72	5.3 mmol	1.00 mL, 10.6 mmol		200 °C, 72 h
ZNP-Ac ₂ O 200/168				200 °C, 168 h
ZNP-Ac ₂ O 240/72				240 °C, 72 h
ZNP-Ac ₂ O 270/72				270 °C, 72 h
ZNP-BnOH 200/24	$\text{Zr}(\text{OnPr})_4$	Benzyl alcohol	O-donor	200 °C, 24 h
ZNP-BnOH 200/168	5.3 mmol	10.0 mL, 96 mmol		200 °C, 168 h
ZNP-BnOH 240/24				240 °C, 24 h
ZNP-AcPh 200/12	$\text{Zr}(\text{OnPr})_4$	Acetophenone	O-donor	200 °C, 12 h
ZNP-AcPh 240/18	5.3 mmol	10.0 mL, 85.4 mmol		240 °C, 18 h
ZNP-MPK 200/12	$\text{Zr}(\text{OnPr})_4$	2-pentanone	O-donor	200 °C, 12 h
ZNP-MPK 200/72	5.3 mmol	10.0 mL, 94 mmol		200 °C, 72 h
ZNP-MPK 200/168				200 °C, 168 h
ZNP-MPK 240/18				240 °C, 18 h
ZNP-MPK 240/72				240 °C, 72 h
ZNP-ACE 200/12	$\text{Zr}(\text{OnPr})_4$	Acetone	O-donor	200 °C, 12 h
ZNP-ACE 240/72	5.3 mmol	10.0 mL, 135 mmol		240 °C, 72 h
ZCL-DIPE 110/72	ZrCl_4	Diisopropylether	CH_2Cl_2 , 10 mL	110 °C, 72 h
ZCL-DIPE 180/72	8.0 mmol	17.6 mmol		180 °C, 72 h
ZCL-EtOH 110/72	ZrCl_4	Ethanol, 6.0 mL, 103 mmol	O-donor	110 °C, 72 h
ZCL-EtOH 150/72	8.0 mmol			150 °C, 72 h
ZCL-BnOH 110/12	ZrCl_4	Benzyl alcohol	O-donor	110 °C, 12 h
ZCL-BnOH 180/12	8.0 mmol	6.7 mL, 64 mmol		180 °C, 12 h
ZCL-ACE 200/18	ZrCl_4	Acetone	O-donor	200 °C, 18 h
ZCL-ACE 240/72	8.0 mmol	10 mL, 135 mmol		240 °C, 72 h

aqueous: the reaction of ZrCl_4 with DIPE at 110 or 180 °C, of $\text{Zr}(\text{OnPr})_4$ with Ac_2O at 200 °C, and of $\text{Zr}(\text{OnPr})_4$ in BnOH at 200 °C. Conversely, the reaction of ZrCl_4 in EtOH, BnOH or acetone and the reactions of $\text{Zr}(\text{OnPr})_4$ in the different ketones at 240 °C all led to rather high water content, between 3500 and 19000 ppm. In these cases, the $\text{H}_2\text{O}:\text{Zr}$ ratio in the syneresis liquid after reaction ranges from 0.20 to 1.75 (Table 2), which is far from negligible, especially considering that this is the amount of water present after reaction, and that hydrolysis/condensation reactions could have consumed a significant amount of water (up to 2 moles per mole of Zr precursor for a completely hydrolytic pathway).

Structure of ZrO_2 samples

The peaks found in the XRD patterns (Figures 1 and 2) of the crystalline samples can be ascribed either to the tetragonal phase, t- ZrO_2 (space group $P42/nmc$, ICSD 00-050-1089) (peaks at $2\theta = 30.3^\circ, 34.8^\circ, 35.3^\circ, 50.4^\circ, 59.6^\circ, 60.2^\circ$) or to the monoclinic phase m- ZrO_2 (space group $P21/a$, ICSD 00-037-1484) (peaks at $2\theta = 24.0^\circ, 24.4^\circ, 28.2^\circ, 31.5^\circ, 34.2^\circ, 34.4^\circ, 35.3^\circ$). The t- ZrO_2 phase is very close to the cubic phase, c- ZrO_2 (space group $Fm\bar{3}m$, ICSD 00-049-1642) and in some case line broadening

can make the assignment difficult. However, the asymmetry of the $\kappa\alpha_1$ peaks at $2\theta = 35^\circ$ and 60° , due to the characteristic splittings of the tetragonal phase, supports a tetragonal structure.^[36] The volume percentage of tetragonal phase, %t, was derived from the intensities of the (101) peak of t- ZrO_2 at 30.3° and of the (−111) and (111) peaks of m- ZrO_2 at 28.2 and 31.5°, respectively.^[37]

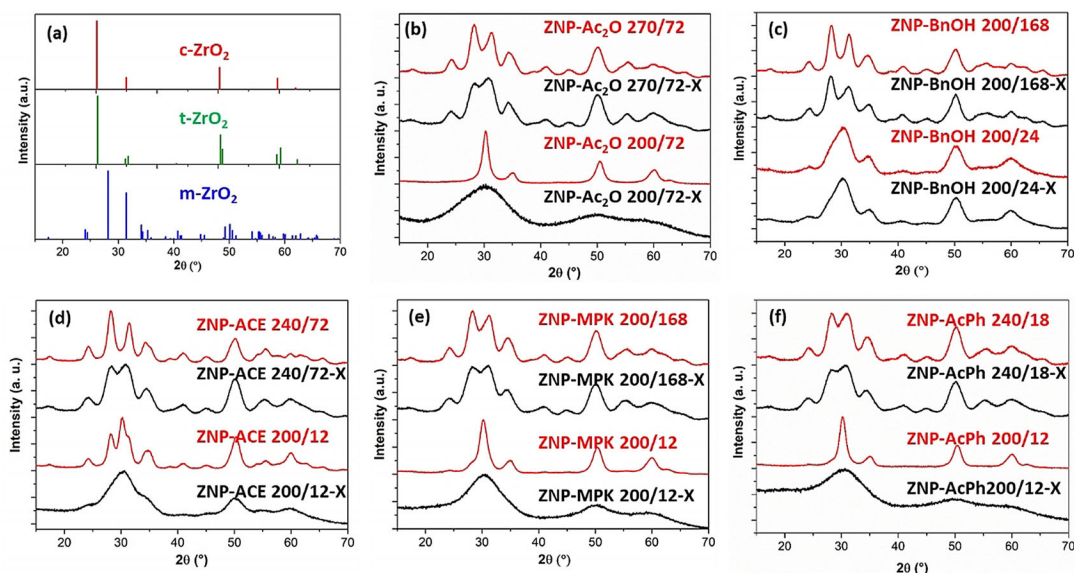
The data reported in Table 2 show that for both precursors, ZrCl_4 and $\text{Zr}(\text{OnPr})_4$, several sets of reaction conditions (O-donor, reaction temperature and time) lead after calcination to practically pure t- ZrO_2 (%t ≥ 95) (e.g. ZNP-Ac₂O 200/72, ZNP-AcPh 200/12, ZCL-DIPE 110/72, ZCL-BnOH 110/12) or practically pure m- ZrO_2 (%t ≤ 5) (e.g. ZNP-ACE 240/72, ZCL-EtOH 150/72, ZCL-BnOH 180/12, ZCL-ACE 200/18, ZNP-BnOH 200/168).

Comparison of the diffractograms of the different samples before and after calcination (Figures 1 and 2) shows that under our conditions (5 h at 500 °C in air) calcination has a significant impact only for the amorphous samples (e.g. ZNP-Ac₂O 200/72, ZNP-MPK 200/12, ZNP-AcPh 200/12, ZCL-DIPE 110/72, ZCL-EtOH 110/72, ZCL-BnOH 110/12), which are converted upon calcination to predominantly tetragonal samples. Calcination of crystalline xerogels only leads to a moderate change (< 10%) of the percentages of tetragonal and monoclinic phases.

Table 2. Crystalline phases and specific surface area of the non-hydrolytic zirconia samples, before and after calcination, and water content in the liquid phase after reaction.

Sample name	% t ^[a] (vol %)		$S_{\text{BET}}^{\text{[b]}}$ ($\text{m}^2 \text{ g}^{-1}$)		H ₂ O	H ₂ O:Zr ^[d]
	xerogel	calcined	xerogel	calcined	ppm ^[c]	
ZNP-Ac ₂ O 200/12	Am. ^[e]	100	500	< 5	< 10	0.00
ZNP-Ac ₂ O 200/72	Am.	100	250	< 5	< 10	0.00
ZNP-Ac ₂ O 200/168	Am.	100	/	< 5	< 10	0.00
ZNP-Ac₂O 240/72	20	15	310	80	890	0.10
ZNP-Ac ₂ O 270/72	20	10	445	95	940	0.11
ZNP-BnOH 200/24	35	45	< 5	20	40	0.00
ZNP-BnOH 200/168	5	5	< 5	5	70	0.01
ZNP-BnOH 240/24	70	75	45	55	1160	0.14
ZNP-ACE 200/12	40	45	470	55	9460	0.91
ZNP-ACE 240/72	15	5	230	85	18700	1.75
ZNP-AcPh 200/12	Am.	95	105	40	450	0.06
ZNP-AcPh 240/18	15	15	210	95	9460	1.13
ZNP-MPK 200/12	Am.	90	225	80	410	0.04
ZNP-MPK 200/72	70	65	375	80	2860	0.28
ZNP-MPK 200/168	20	15	275	110	6430	0.62
ZNP-MPK 240/18	25	20	260	95	7670	0.74
ZNP-MPK 240/72	20	15	235	115	15400	1.48
ZCL-DIPE 110/72	Am.	100	20	95	< 10	0.00
ZCL-DIPE 180/72	100	100	< 5	10	< 10	0.00
ZCL-EtOH 110/72	Am.	85	/	40	3500	0.14
ZCL-EtOH 150/72	5	5	160	130	11500	0.45
ZCL-BnOH 110/12	Am.	85	/	130	610 ^[f]	0.30
ZCL-BnOH 180/12	15	5	100	80	H ₂ O phase	/
ZCL-ACE 200/18	5	0	100	105	H ₂ O phase	/
ZCL-ACE 240/72	0	0	/	70	H ₂ O phase	/

[a] Volume percentage of t-ZrO₂ phase, values rounded to the nearest 5% (% m = 100 – % t). [b] Specific surface area obtained by the BET method. [c] From Karl Fischer titration of the liquid phase. [d] Water to Zr molar ratio calculated from the water content and the amounts of reactants, assuming complete condensation and assuming that all the water and organic byproducts are in the liquid phase. [e] Amorphous. [f] No syneresis liquid, the gel was crushed under argon in 6.0 mL anhydrous EtOH and the ethanolic solution was analyzed.

**Figure 1.** Reference XRD patterns for monoclinic, tetragonal, and cubic zirconia polymorphs (a), and powder XRD patterns of selected samples prepared from Zr(OnPr)₄, before (black) and after calcination (red) (b–f).

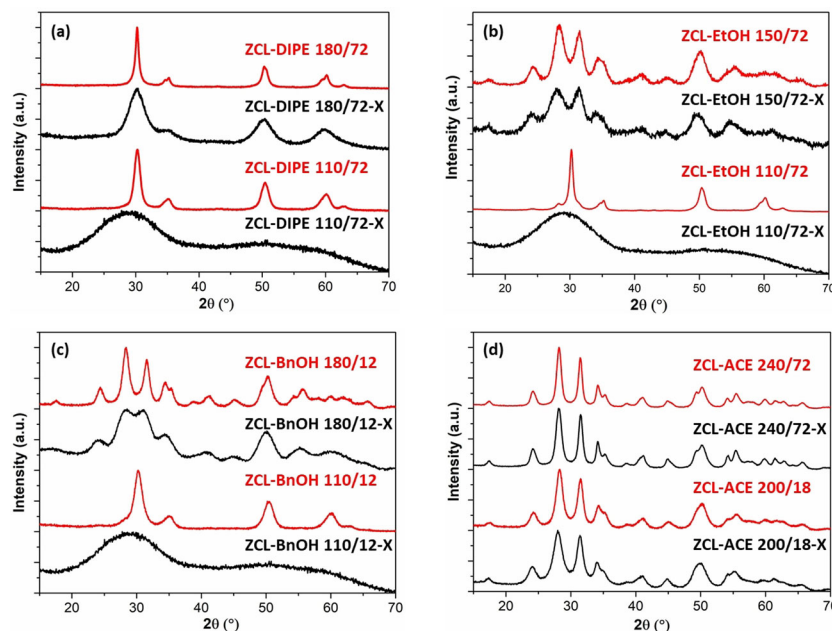


Figure 2. Powder XRD patterns of selected ZrO_2 samples prepared from ZrCl_4 , before (black) and after calcination (red) (a–d).

Texture of ZrO_2 samples

Before calcination, the specific surface areas (S_{BET}) range between 0 and $500 \text{ m}^2 \text{ g}^{-1}$, and after calcination, between 0 and $130 \text{ m}^2 \text{ g}^{-1}$. There is no correlation between the water content in the reaction medium and S_{BET} of the xerogels. In most cases calcination leads to a significant decrease of S_{BET} . This decrease can be due to crystallite growth, resulting in a lower geometrical surface area of the particles, and to the sintering of the particles. Significant particle growth upon calcination occurs for instance in ZNP- Ac_2O 270/72, ZNP-ACE 240/72 or ZCL-BnOH 180/12, as shown by the narrowing of XRD peaks upon calcination (Figures 1 and 2). Conversely, the removal of organic residues by the calcination should lead to an increase in the specific surface area, as organics are usually non porous and may partially block the pores. Due to these conflicting effects, predicting the effect of calcination on specific surface areas is not possible.

Note that the calcination step was not optimized in view of obtaining very high surface areas. In all cases the samples were calcined at 500°C for 5 h (heating rate $10^\circ\text{C min}^{-1}$). A lower calcination temperature and/or a shorter calcination time could lead to significantly higher surface areas. For instance, we found that calcination at 500°C for 1 h instead of 5 h of ZNP- Ac_2O 240/72 and ZCL-BnOH 180/12 led to nearly twice higher specific surface areas and higher pore volumes, while a low heating rate (1°C min^{-1} instead of $10^\circ\text{C min}^{-1}$) had nearly no influence (Table S1 and Figure S2).

Even after calcination at 500°C for 5 h, several syntheses led to nearly pure m- ZrO_2 or t- ZrO_2 with high specific surface area. With the $\text{Zr}(\text{OnPr})_4$ precursor, reaction with ketones appear particularly interesting, thus reaction with MPK at 200°C for 12 h mainly leads to t- ZrO_2 (%t = 90%) with a S_{BET} of $80 \text{ m}^2 \text{ g}^{-1}$ while reaction with ACE at 240°C for 72 h affords nearly pure

m- ZrO_2 (%t = 5%) with a S_{BET} of $85 \text{ m}^2 \text{ g}^{-1}$. In the case of the ZrCl_4 precursor, reaction with DIPE at 110°C for 72 h leads to pure t- ZrO_2 with a S_{BET} of $95 \text{ m}^2 \text{ g}^{-1}$ while reaction in EtOH at 150°C for 72 h leads to m- ZrO_2 (%t = 5%) with a S_{BET} of $130 \text{ m}^2 \text{ g}^{-1}$ (samples highlighted in bold in Table 2). The texture and morphology of these samples are presented in part 3.4.

Part 2: Control of the crystalline phase

In several cases, we could control the crystalline phase of the calcined samples and obtain either nearly pure t- ZrO_2 or nearly pure m- ZrO_2 simply by changing the reaction time and/or the reaction temperature (Figures 1, 2).

Increasing the reaction time or the reaction temperature tends to favor the formation of m- ZrO_2 at the expense of t- ZrO_2 , suggesting that the metastable tetragonal forms first then transforms into the stable monoclinic phase during the solvothermal aging of the gel (e.g. ZNP-BnOH 200/12 vs. ZNP-BnOH 200/168, ZNP-MPK 200/12 vs. ZNP-MPK 200/168, ZNP- Ac_2O 200/72 vs. ZNP- Ac_2O 240/72, ZCL-EtOH 110/72 vs. ZCL-EtOH 150/72, ZCL-BnOH 110/72 vs. ZCL-BnOH 180/72).

However, in the reaction of ZNP with Ac_2O at 200°C , t- ZrO_2 formed whatever the reaction time (12 h to 168 h), and in the reaction of ZCL with DIPE, pure t- ZrO_2 was obtained regardless of the reaction temperature (110°C or 180°C). It is noteworthy that no water was detected for all of these samples. Actually, although reaction temperature and reaction time are important parameters, the presence of water in the reaction medium has an even more important influence on the crystallinity of the final ZrO_2 . There is a clear correlation between the crystalline phase of the calcined ZrO_2 samples and the amount of water found after reaction. Thus, it is remarkable that strictly non-hydrolytic syntheses ($\text{ZrCl}_4/\text{DIPE}$ and $\text{Zr}(\text{OnPr})_4/\text{Ac}_2\text{O}$ at 200°C) led in all cases to purely tetragonal samples (ZCL-DIPE

110/72, ZCL-DIPE 180/72, ZNP-Ac₂O 200/12, ZNP-Ac₂O 200/72, ZNP-Ac₂O 200/168) and that all the reactions with large amounts of water (>1500 ppm) led to predominantly monoclinic samples (%t ≤ 40).

The presence of a significant amount of water in the synthesis liquid after reaction suggests that the formation of the oxide involves, at least in part, hydrolysis/condensation reactions (see paragraph on mechanisms). In addition, water might also play a role during the solvothermal aging of the gel by facilitating the conversion of tetragonal zirconia to monoclinic zirconia.

Solvothermal aging in the presence of water

To investigate the influence of a small amount of water on the solvothermal aging of the gel, we repeated two reactions which led to predominantly tetragonal zirconia (%t ≥ 80): the reactions of Zr(OnPr)₄ and Ac₂O in toluene at 200 °C for 36 h (ZNP-Ac₂O 200/36) and of Zr(OnPr)₄ in MPK at 200 °C for 12 h (ZNP-MPK 200/12). The gels issued from these reactions were washed, then heated in an autoclave at 200 °C in toluene containing 20000 ppm H₂O. The resulting xerogels and calcined samples (ZNP-Ac₂O 200/36-W200/36 and ZNP-MPK 200/12-W200/12) were characterized by powder X-ray diffraction and the results are given in Table 3 and Figure 3.

Table 3. Influence of a solvothermal treatment in 10 mL toluene containing 2 wt % H ₂ O on the crystalline phases before and after calcination.			
Sample	Solvothermal treatment	%t ^[a] [vol%] xerogel	%t ^[a] [vol%] after calc.
ZNP-Ac ₂ O 200/72	None	Am.	100
ZNP-Ac ₂ O 200/36-W200/36	36 h at 200 °C	5	5
ZNP-MPK 200/12	None	Am.	90
ZNP-MPK 200/12-W200/12	12 h at 200 °C	35	10

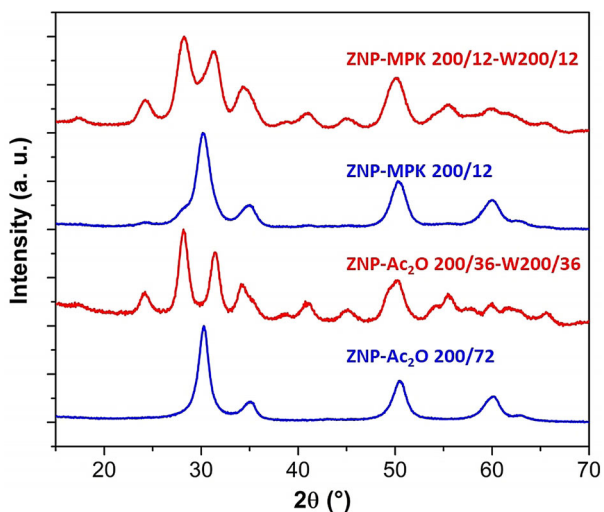


Figure 3. Comparison of the powder XRD patterns of calcined ZrO₂ samples prepared with (red) or without (blue) a solvothermal treatment with 2 wt % of added water.

In the case of the strictly nonhydrolytic reaction of Zr(OnPr)₄ with Ac₂O at 200 °C, we know that an amorphous xerogel is obtained whatever the reaction time (12 h to 168 h), and that this xerogel is converted after calcination into a purely tetragonal sample. Remarkably, a solvothermal treatment of 36 h at 200 °C in toluene with only 2 wt% H₂O is sufficient to convert the amorphous gel into nearly pure m-ZrO₂ (%t ≤ 5). A similar effect is observed in the reaction of Zr(OnPr)₄ with MPK at 200 °C for 12 h: after a solvothermal treatment of only 12 h at 200 °C in the presence of H₂O m-ZrO₂ becomes the major phase in both the xerogel and the final oxide.

In both cases, the presence of water clearly favors the formation of monoclinic ZrO₂, even though the crystallite size (8.5 nm for ZNP-Ac₂O 200/36-W200/36, 5.5 nm for ZNP-MPK 200/12-W200/12) remains well below the critical particle size (=30 nm) defined by Garvie and Goss.^[17] Gambe and co-workers recently reported that a solvothermal post-treatment in mixtures of BnOH and H₂O of wet ZrO₂ particles obtained by the benzyl alcohol route also favored the monoclinic phase without significant particle growth.^[34] This behavior could be explained by a preferential lowering of the surface free energy of m-ZrO₂ particles upon adsorption of water, leading to a decrease of the critical size below which t-ZrO₂ particles can be stabilized,^[24] or to the filling of oxygen vacancies by hydroxyl ions.^[38]

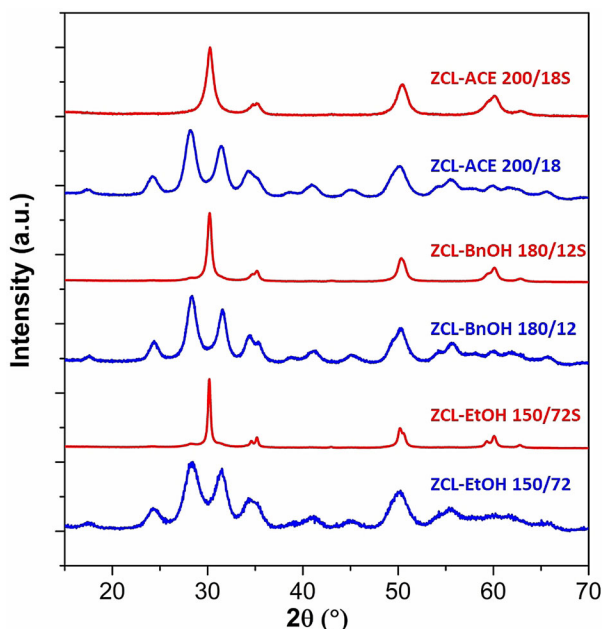
Avoiding water formation

It is easy to add water, much less to remove it during the reaction, considering that the syntheses are performed in autoclaves. Recently, Gambe et al. demonstrated that by adding sodium as a desiccant in the reaction of benzyl alcohol with Zr(O*i*Pr)₄-iPrOH they could obtain pure t-ZrO₂ nanoparticles instead of t/m mixtures.^[34] Actually, in all the reactions leading to large amounts of water, the O-donor is also used as a solvent, thus in a large excess. In the case of ZrCl₄ the only source of oxygen is the O-donor. An elegant way to avoid the formation of water would be to use a stoichiometric amount of O-donor, that is, 2 equiv relative to ZrCl₄. Then, all the oxygen would be consumed to give the oxo bridges and, whatever the reactions involved, no water should remain in the reaction medium. To test this hypothesis, we chose three reactions of ZrCl₄ with EtOH, BnOH or ACE, which lead, when the O-donor is used as a solvent, to large amounts of water and to nearly pure m-ZrO₂ (%t ≤ 5). Three samples were prepared under the same conditions but using an inert solvent and a stoichiometric amount (i.e. 2 equiv relative to Zr) of O-donor (Table 4).

With a stoichiometric amount of O-donor, the amount of water found in the liquid phase was very low (<100 pm) and the major phase in the calcined samples was the tetragonal one (%t ≥ 85) (Table 4, Figure 4). The very low amount of water found confirms that even if water formed intermediately, it was completely consumed to form the ZrO₂ gel. The fact that the major phase was the tetragonal one is consistent with our previous observations and confirms that in the absence of water the tetragonal phase remains stabilized and formation of monoclinic zirconia is hindered.

Table 4. Crystalline phases before and after calcination for zirconia samples prepared from ZrCl_4 (8.0 mmol) with a stoichiometric amount (16.0 mmol) of ACE, EtOH or BnOH O-donors.

Sample name	O-donor	Solvent	Conditions	H_2O [ppm]	xerogel	%t ^[a] [vol%] after calc.
ZCL-EtOH 150/72S	EtOH	CH_2Cl_2 , 10 mL	150 °C, 72 h	60	Am.	80
ZCL-BnOH 180/12S	BnOH	Toluene, 10 mL	180 °C, 12 h	50	Am.	85
ZCL-ACE 200/18S	ACE	CH_2Cl_2 , 10 mL	240 °C, 72 h	30	Am.	100

**Figure 4.** Comparison of the powder XRD patterns of calcined ZrO_2 samples prepared from ZrCl_4 with a stoichiometric amount of O-donor (red) or using the O-donor in large excess as a solvent (blue).

Taken together, our findings underline the crucial importance of water on the crystalline phase of the final ZrO_2 , which apparently does not depend so much on the mechanism of

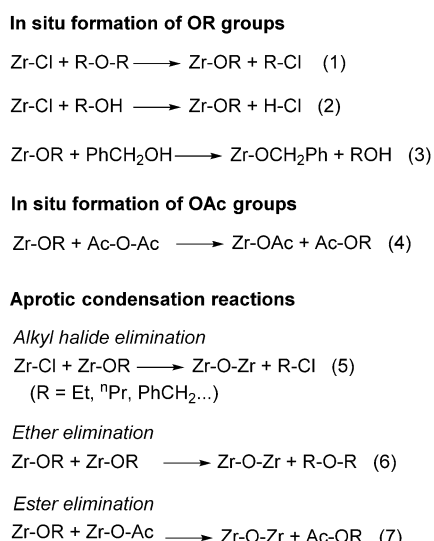
gel formation (strictly nonhydrolytic or not) than on the presence of water during the solvothermal aging of the gel. Thus, it is possible to reverse the selectivity of syntheses either by adding a small amount of water during the solvothermal aging of the gels or by using a stoichiometric amount of O-donor to prevent the formation of water.

Part 3: Reactions involved

Having established the main parameters controlling the crystalline phase in the final ZrO_2 samples and the crucial role played by water, we used ^1H and ^{13}C NMR spectroscopy to identify organic reaction products, in order to determine the reactions responsible for the formation of the oxide network and for the formation of water. The reaction of $\text{Zr}(\text{OnPr})_4$ with acetophenone (AcPh) or 2-pentanone (MPK) at 200 or 240 °C led to complicated mixtures of products, hence we focused on the reactions with the simplest ketone, acetone (ACE). The NMR spectra are displayed in supporting information. The different reactions that we propose are summarized in Scheme 1.

Strictly non-hydrolytic syntheses

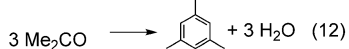
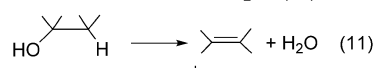
The quantification of water in the syneresis liquid (Table 2) indicates that very few syntheses can be considered as strictly non-hydrolytic: the reaction of ZrCl_4 with DIPE at 110 or 180 °C,



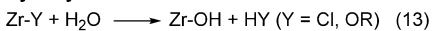
Non-hydrolytic hydroxylation



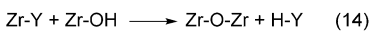
Water formation



Hydrolysis



Condensations involving M-OH groups

**Scheme 1.** Main reactions proposed for the formation of the oxide network and of water.

of $\text{Zr}(\text{OnPr})_4$ with Ac_2O at 200°C , and of $\text{Zr}(\text{OnPr})_4$ in BnOH at 200°C .

Reaction of ZrCl_4 with DIPE: After reaction of ZrCl_4 with DIPE (2.2 equiv) at 110°C for 72 hours in CH_2Cl_2 (ZCL-DIPE 110/72), NMR spectra indicate the presence of isopropyl chloride (88 mol%) and $i\text{Pr}_2\text{O}$ (12 mol%) (Figure S3). The formation of isopropyl chloride is consistent with a 2-step mechanism involving first the formation of Zr-O*i*Pr groups by etherolysis [Eq. (1) in Scheme 1] then their aprotic condensation with Zr-Cl groups [Eq. (5)]. The 12 mol% of $i\text{Pr}_2\text{O}$ correspond to unreacted excess $i\text{Pr}_2\text{O}$. The same strictly nonhydrolytic mechanism has been reported for the synthesis of TiO_2 ^[39,40] and TiO_2/C nanocomposites from TiCl_4 and DIPE.^[41] In addition, very minor signals between 0.7 and 2.0 ppm suggest the presence of alkyl oligomers, likely resulting from the formation of propylene by dehydrochlorination of $i\text{PrCl}$, followed by polymerization.^[39,41]

Reaction of $\text{Zr}(\text{OnPr})_4$ with Ac_2O at 200°C : After reaction of $\text{Zr}(\text{OnPr})_4$ with 2 equiv of Ac_2O at 200°C for 72 h (ZNP-Ac₂O 200/72), NMR spectra indicate the formation of n-propyl acetate (AcOnPr) only (Figure S4), consistent with a 2-step mechanism involving acetoxylation [Eq. (4)] then condensation with ester elimination [Eq. (7)], as recently reported for the synthesis of TiO_2 -based materials from $\text{Ti}(\text{O}i\text{Pr})_4$ and Ac_2O .^[42,43] There is no trace of Ac_2O , showing that the first step was complete. At 240°C , the reaction of ZNP with Ac_2O is no more strictly nonhydrolytic, as shown by the significant amount of water (= 900 ppm) found after reaction at 240°C or 270°C for 72 h (samples ZNP-Ac₂O 240/72 and ZNP-Ac₂O 270/72), possibly related to the decomposition of $\text{Zr}(\text{OnPr})_4$ [Eq. (8)] followed by condensation with elimination of H_2O [Eq. (15)].^[44]

Reaction of $\text{Zr}(\text{OnPr})_4$ with BnOH at 200°C : After reaction of $\text{Zr}(\text{OnPr})_4$ with BnOH at 200°C (ZNP-BnOH 200/168) the ^{13}C NMR spectrum (Figure S5) clearly shows the formation of n-propanol ($n\text{PrOH}$), and dibenzyl ether (Bn_2O). Unfortunately, the ^1H NMR resonances for BnOH and Bn_2O overlap, preventing integration. The formation of Bn_2O and $n\text{PrOH}$ is in good agreement with the nonhydrolytic mechanism previously reported in the synthesis of ZrO_2 ^[33] or TiO_2 ^[7] nanoparticles, involving transesterification [Eq. (3)] then aprotic condensation with ether elimination [Eq. (6)]. Again, this reaction is no more strictly non-hydrolytic when it is performed at 240°C (1160 ppm). The spectra obtained for the sample ZNP-BnOH 240/24 (Figure S6) are quite similar to those of ZNP-BnOH 200/168, although many minor peaks are now visible. Accordingly, the formation of water could result from the intermolecular dehydration of BnOH to give BnOBn [Eq. (10)],^[7] or from the intramolecular dehydration of $n\text{PrOH}$ [Eq. (11)], with formation of propylene, which is too volatile to be detected.^[34]

Syntheses with *in situ* formation of water

As discussed above, significant water formation is observed notably in the reactions of ZNP or ZCL in acetone at $200\text{--}240^\circ\text{C}$, and in the reaction of ZCL in ethanol at 150°C or in benzyl alcohol at 180°C (Table 2).

Reaction of $\text{Zr}(\text{OnPr})_4$ in acetone: After reaction at 240°C for 72 h (sample ZNP-ACE 240/72): the ^1H and ^{13}C NMR spectra

(Figure S7) show the formation of mesitylene, isopropanol ($i\text{PrOH}$), and minor amounts of saturated hydrocarbons (peaks between 0.6 and 2 ppm), as well as other unidentified by-products. The molar ratio mesitylene : $i\text{PrOH}$: ACE is 1:3.5:19. Minor formation of mesitylene has previously been reported in the synthesis of TiO_2 nanoparticles from $\text{Ti}(\text{O}i\text{Pr})_4$ and acetone,^[7,45] the major product being mesityl oxide. Both compounds result from aldol condensation of acetone [Eq. (12)]. In our case, the preferential formation of the higher condensation product, mesitylene, suggests that Zr species are more selective catalysts for this reaction than Ti species. Considering the high amount of water in the medium, it is likely that hydrolysis of Zr-OnPr groups to Zr-OH groups [Eq. (13)] and condensation with Zr-OnPr groups [Eq. (14)] or other Zr-OH groups [Eq. (15)] take place. Both hydrolysis [Eq. (13)] and condensation according to [Eq. (14)] should generate *n*-propanol. The fact that only isopropanol was detected suggests that isomerization of *n*-propanol took place, which has to be ascribed the harsh reaction conditions used. For comparison, the synthesis of mesitylene from acetone typically involves reacting acetone in concentrated sulfuric acid or heating over an acidic catalyst at high temperature ($> 200^\circ\text{C}$) and high pressure.^[46,47]

Reaction of ZrCl_4 in acetone at 200°C : After 18 h (sample ZCI-ACE 200/18), both ^1H and ^{13}C NMR spectra (Figure S8) point to the complete consumption of the acetone. The major byproduct is mesitylene (as in the reaction of $\text{Zr}(\text{OnPr})_4$ in acetone), indicating extensive aldol condensation and water formation [Eq. (12)], in agreement with the water phase found in the syneresis liquid. In addition, numerous signals corresponding to saturated aliphatic and aromatic byproducts are found. These byproducts most likely arise from the polymerization of light olefins formed by decomposition of mesityl oxide and other aldol condensation products, which was reported to be catalyzed by Brønsted acidic sites in zeolites at $150\text{--}250^\circ\text{C}$ and leads to the formation of isobutylene, but also of propylene, ethylene and aromatics.^[48] Actually, light olefin synthesis from acetone over zeolite catalysts in gas phase has been widely investigated. In these syntheses, selective formation of lighter olefins is due to the molecular sieving effect of the zeolite.^[49] In our case, there is no such effect and polymerization is not prevented.

Reaction of ZrCl_4 in EtOH at 150°C : After 72 h of reaction (sample ZCL-EtOH 150/72), NMR spectra indicate the formation of Et_2O and EtCl only (Figure S9). From the integration of the ^1H NMR spectrum and the initial molar ratio of reactants ($\text{EtOH}:\text{ZrCl}_4 = 12.9:1$), we find that 2.6 moles of Et_2O and 1.6 moles of EtCl were produced for one mole of ZrCl_4 . The formation of water (11500 ppm) and Et_2O most likely results from the condensation between two EtOH molecules [Eq. (10)], catalyzed by Zr species and/or HCl. This reaction is relatively slow: over the 72 h of reaction, less than half the EtOH was converted to Et_2O , nevertheless generating more than enough water to fully hydrolyze and condense the precursor. However, the presence of EtCl suggests that a nonhydrolytic mechanism involving alkoxylation [Eq. (2)] and condensation with EtCl elimination [Eq. (5)] is operative.

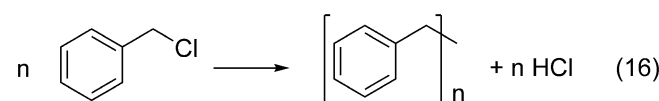
According to the literature, the alkoxylation starts even at room temperature but this reaction is not complete and leads to the formation of a mixture of chloroethoxides, mainly $\text{Zr}(\text{OEt})_2\text{Cl}_2\text{-EtOH}$ and $\text{Zr}(\text{OEt})\text{Cl}_3\text{-EtOH}$.^[50] At 150 °C, these chloroethoxides condense rapidly to form Zr-O-Zr bonds according to [Eq. (5)]. The amount of EtCl formed ($\text{EtCl:Zr} = 1.6:1$) corresponds to 80% of the amount expected for a complete nonhydrolytic condensation. Accordingly, only about 20% of the oxo bridges would be formed by a hydrolytic mechanism [Eqs. (13–15)].

Interestingly, when the reaction was performed using a stoichiometric amount of EtOH, that is, 2 moles per mole of ZrCl_4 (sample ZCl-EtOH 150/72S), no water was detected (meaning that all the EtOH was consumed to give alkoxide groups, [Eq. (2)] and the only byproduct detected by ^1H and ^{13}C NMR spectroscopy of the syneresis liquid was EtCl (Figure S10) suggesting that all of the oxo bridges formed according to [Eq. (5)], by a fully nonhydrolytic mechanism. As a result, the solvothermal “aging” takes place under anhydrous conditions, leading to an amorphous ZrO_2 xerogel converted to t-ZrO₂ upon calcination.

Reaction of ZrCl_4 in BnOH : After reaction of ZrCl_4 in BnOH at 110 °C for 12 h (sample ZCl-BnOH 110/12), there was no syneresis liquid. To extract organic byproducts and water, the gel was crushed under argon in anhydrous EtOH. Karl Fischer titration of this ethanolic solution indicated the formation of a significant amount of water (6 100 ppm). Besides EtOH, The ^1H and ^{13}C NMR spectra of the resulting solution (Figure S11) clearly show the presence of BnOH , BnCl and Bn_2O . Based on the integration of the ^1H NMR spectrum and the initial molar ratio of reactants, about 70% of the benzyl alcohol was consumed during the reaction, 30% to give BnCl and 40% to form Bn_2O . The formation of BnCl could result from an alkoxylation/condensation process [Eq. (2) and (5)] but it is more probably due to the nonhydrolytic hydroxylation of Zr-Cl groups [Eq. (9)], which is favored over alkoxylation in the case of tertiary and benzylic alcohols, able to form stable carbocations.^[3,7] The Zr-OH groups formed by this nonhydrolytic hydroxylation would then condense according to [Eq. (14)] or [Eq. (15)], leading to the elimination of HCl or water, respectively. The formation of Bn_2O most likely results from the dehydration between two BnOH molecules [Eq. (10)], catalyzed by Zr species and/or HCl.

Reaction at 180 °C (sample ZCl-BnOH 180/12) also leads to BnCl , Bn_2O and H_2O , indicating the occurrence of the same reactions as at 110 °C (Figure S12). In addition, other side reactions take place, leading to short poly(phenylene methylene) oligomers. The formation of such oligomers has previously been reported in the reaction of benzyl alcohol with iron^[51,52] or tungsten precursors.^[53] Poly(phenylene methylene) may result from the direct polymerization of BnOH , but also of BnCl or Bn_2O byproducts.^[7] Close inspection of the ^1H NMR spectrum shows the presence of CH_2Cl chain ends, indicating that BnCl did participate to the polymerization [Eq. (16)].^[54] According to the integration of the ^1H NMR spectrum, more than 90% of the benzyl alcohol was converted during the reaction,

43% to BnCl , 23% to Bn_2O and 25% to poly(phenylene methylene) oligomers.



Part 4: Texture and morphology of selected samples

Based on their phase purity and their specific surface area, we selected four samples for further characterization: two samples with a predominantly monoclinic structure (ZCL-EtOH 150/72 and ZNP-ACE 240/72), and two samples with a predominantly tetragonal structure (ZCL-DIPE 110/72 and ZNP-AcPh 200/12). In addition, to illustrate the evolution of the texture with reaction conditions, we also selected samples prepared from ZNP and Ac₂O at different temperatures (200, 240, and 270 °C) for 72 h, and samples prepared from ZNP and MPK at 200 °C with different reaction times (12, 72, and 168 h). Relevant structural and textural data for these samples are given in Table 5.

Table 5. XRD and N_2 physisorption data for the selected ZrO_2 samples.

Sample	Phase ^[a]	$d_{\text{cryst}}^{\text{[b]}}$ [nm]	$S_{\text{geom}}^{\text{[c]}}$ [$\text{m}^2 \text{g}^{-1}$]	$S_{\text{BET}}^{\text{[d]}}$ [$\text{m}^2 \text{g}^{-1}$]	$V_p^{\text{[e]}}$ [$\text{cm}^3 \text{g}^{-1}$]	$D_p^{\text{[f]}}$ [nm]
ZCL-EtOH 150/72	95 % m-ZrO ₂	5.5	180	130	0.30	5.9
ZNP-ACE 240/72	95 % m-ZrO ₂	7.0	140	85	0.17	5.9
ZCL-DIPE 110/72	100 % t-ZrO ₂	9.0	110	95	0.18	6.1
ZNP-MPK 200/12	95 % t-ZrO ₂	6.0	165	80	0.07	3.4
ZNP-MPK 200/72	65 % t-ZrO ₂ / 35 % m-ZrO ₂	6.5 / 5.5	165	80	0.11	4.5
ZNP-MPK 200/168	85 % m-ZrO ₂	5.0	200	110	0.19	5.4
ZNP-Ac ₂ O 200/72	100 % t-ZrO ₂	7.5	135	< 5	< 0.01	/
ZNP-Ac ₂ O 240/72	85 % m-ZrO ₂	6.5	155	80	0.11	4.7
ZNP-Ac ₂ O 270/72	90 % m-ZrO ₂	6.0	165	95	0.36	12.1

[a] Percentage of the main crystalline phase. [b] Average crystallite size for the major phase, determined by the Scherrer method. [c] Geometric specific surface area calculated from the average crystallite size assuming a density of 6 and a spherical shape. [d] Specific surface area obtained by the BET method. [e] Total pore volume at $P/P_0 = 0.98$. [f] Average pore size calculated by the BJH method from the desorption isotherm.

Electron microscopy images show that the calcined samples are built of aggregated primary t- or m-ZrO₂ nanocrystals, between = 5 and 9 nm in size, in good agreement with the crystallite size derived from XRD patterns (Table 5 and Figures 5 and 6). At the micron scale, the samples present two different morphologies depending on the precursor and O-donor: in ZNP-Ac₂O, ZCl-EtOH or ZCL-DIPE samples the nanocrystals form shapeless, very large aggregates, while in ZNP-MPK, ZNP-ACE and ZNP-AcPh they build spherical secondary particles, 1 to 5 μm in size. Similar hierarchical morphologies have already been reported for TiO₂-based materials prepared by NHSG using DIPE or Ac₂O O-donors.^[41,42,55] As shown in Figure 6, these two types of morphologies are already present in the xerogels, prior to calcination.

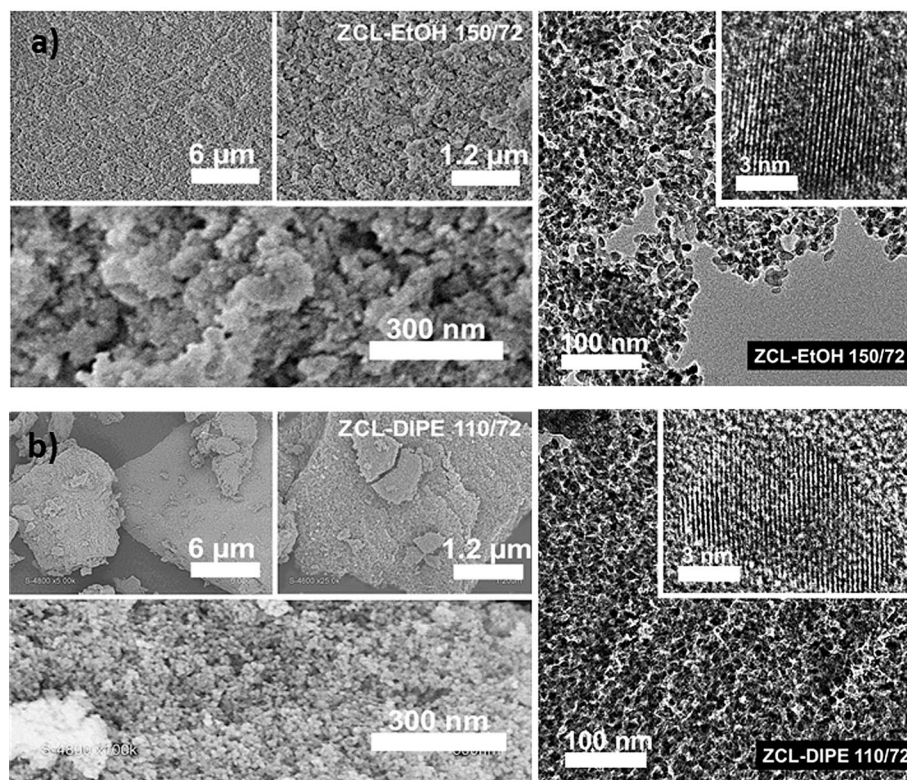


Figure 5. SEM and TEM images for ZCL-EtOH 150/72 (95 % *m*-ZrO₂) (a) and ZCL-DIPE 110/72 (100 % *t*-ZrO₂) (b).

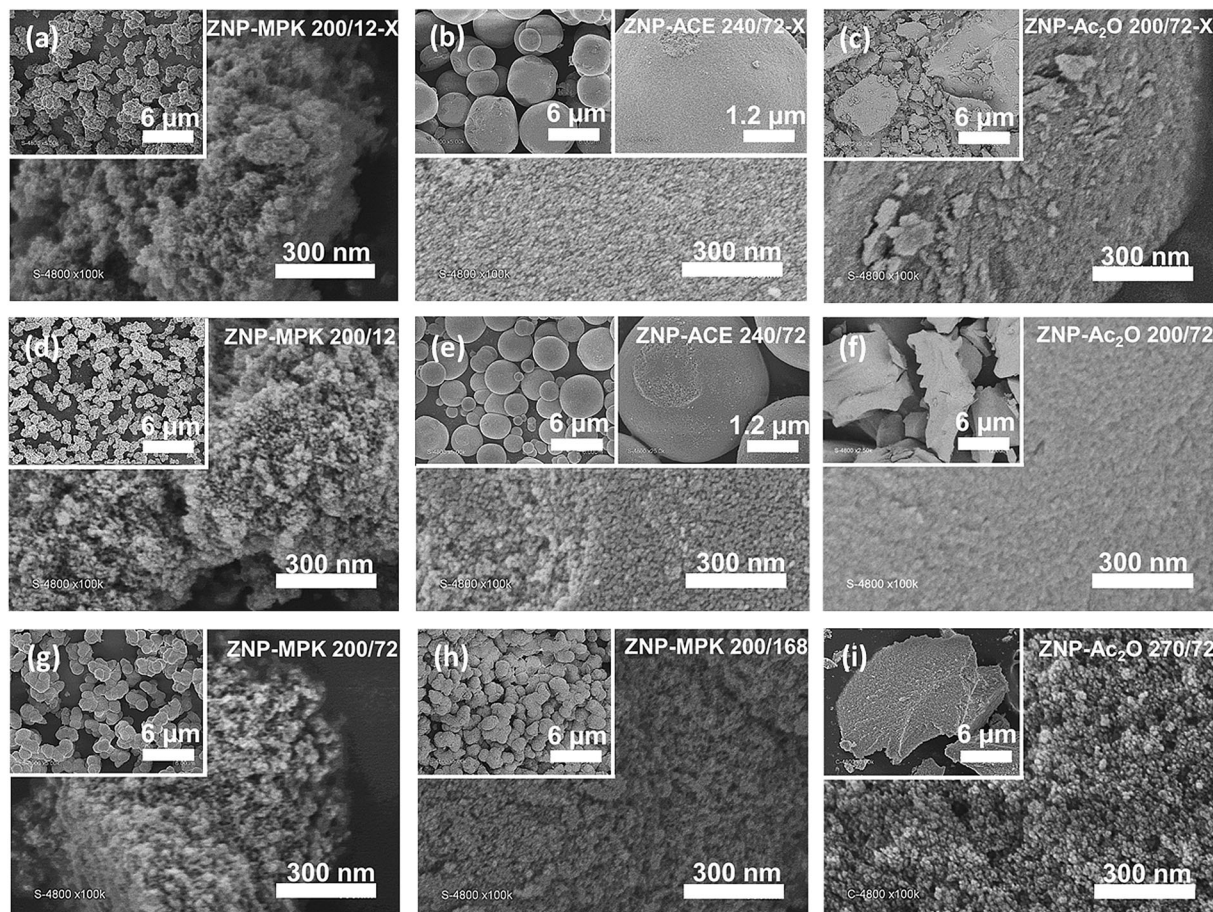


Figure 6. SEM images for ZrO₂ samples obtained from ZNP and MPK, ACE or Ac₂O under different conditions.

The texture of the samples directly depends on how the ZrO_2 nanocrystals assemble in the aggregates during the synthesis, drying and calcination steps. Indeed, these nanocrystals are nonporous, thus the specific surface area (S_{BET}) arises from the accessible geometric surface area (S_{geom}) of the nanocrystals, and the pore volume (V_p) from the voids between them. If there was no sintering of the nanoparticles, the contact area between the NPs would be negligible, and S_{BET} would be close to S_{geom} . In all cases S_{BET} is lower than the geometric surface area, indicating significant sintering of the nanocrystals (Table 5). Sintering appears particularly important for ZNP- Ac_2O 200/72, which displays a very low S_{BET} value despite a particle size of 7.5 nm.

Just as the crystalline phase, the texture depends on the reaction temperature and/or the reaction time. Accordingly, it is not really possible to independently control the structure and the texture of the final oxide. For instance, in the reaction of ZNP with MPK at 200 °C, increasing the reaction time from 12 to 168 h leads to a nearly complete transformation of t- ZrO_2 into m- ZrO_2 . Simultaneously, S_{BET} and V_p increase, from 80 $\text{m}^2 \text{g}^{-1}$ to 110 $\text{m}^2 \text{g}^{-1}$ and from 0.07 $\text{cm}^3 \text{g}^{-1}$ to 0.19 $\text{cm}^3 \text{g}^{-1}$, respectively (Table 5, Figure 7b, c). SEM images (Figure 6) indicate a moderate growth and sintering of the secondary particles. The significant increase in pore volume suggests that the solvothermal aging leads to a stronger primary particles network which resists better to the drying and calcination steps. In the reaction of ZNP with Ac_2O , increasing the reaction temperature from 200 °C to 270 °C changes the structure from pure t- ZrO_2 to nearly pure m- ZrO_2 . This is accompanied by a spectacular increase of S_{BET} (from less than 5 $\text{m}^2 \text{g}^{-1}$ to

95 $\text{m}^2 \text{g}^{-1}$) and of the pore volume (from less than 0.01 $\text{cm}^3 \text{g}^{-1}$ to 0.36 $\text{cm}^3 \text{g}^{-1}$) (Figure 7d). This change in texture is not due to a change in crystallite size, which remains practically constant, but to a lower sintering of the particles, leading to much less dense aggregates, as can be seen in SEM images (Figure 6c, f, i).

The nitrogen physisorption isotherms of the different oxides (Figure 7) are of Type IV, characteristic of mesoporous adsorbents, with Type H2 hysteresis loops, suggesting the presence of ink bottle-shaped pores.^[56] The pore size distributions confirm the presence of mesopores. The distribution is particularly large in the case of ZCL-EtOH 150/72, and to a lesser extent of ZCL-DIPE 110/72. Conversely, the distribution is quite narrow for ZNP-ACE 240/72, which displays well-calibrated pores in the 5 to 7 nm range, due to the relatively dense packing of well-calibrated nanoparticles (Figure 6e). The average pore size in these three samples are similar, around 6 nm. The average pore size of ZNP-MPK 200/12 is much lower (3.4 nm), and the sharp pore size distribution is likely due to cavitation-induced evaporation, indicating the presence of mesopores below ≈ 5 nm.^[56]

Conclusions

The first objective of this work was to assess the in situ formation of water in NHSG routes. Among all the syntheses tested, very few appear strictly non-hydrolytic. This is the case only for the reactions of ZNP with Ac_2O or BnOH at moderate temperature (200 °C) and of ZCL with DIPE, in which no organic reaction produces hydroxyl groups or water and the oxide network

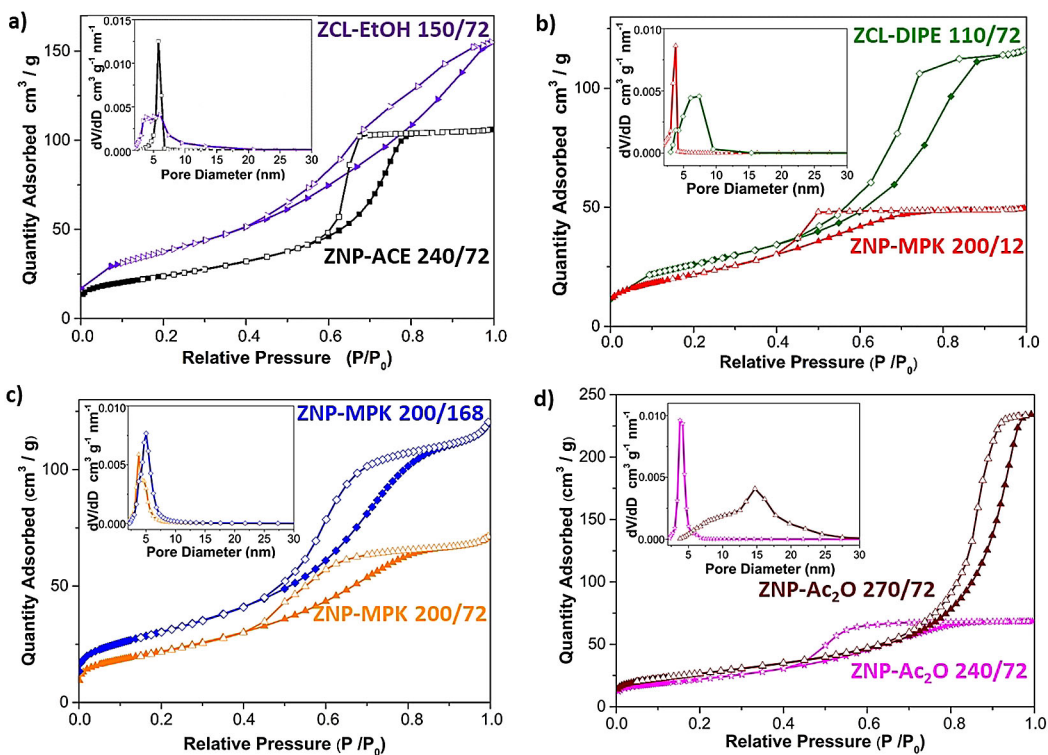


Figure 7. N_2 physisorption isotherms at 77 K and corresponding BJH pore size distribution of selected m- ZrO_2 (a), t- ZrO_2 samples (b), and of additional ZNP-MPK (c) and ZNP- Ac_2O samples (d).

results from aprotic condensations. In all other syntheses, significant water formation takes place via alcohol dehydration (reaction of ZCL with EtOH or BnOH and possibly of ZNP with BnOH at 240 °C) or aldol condensation (reaction of ACE with ZNP or ZCL), suggesting that the mechanism of formation of these samples is, at least in part, hydrolytic.

The second objective was to prepare mesoporous ZrO_2 supports with a controlled tetragonal or monoclinic structure. Although reaction time and reaction temperature were important parameters in controlling the crystalline phase, the presence of water played an even more important role: the formation of t- ZrO_2 is favored in the absence of water, while m- ZrO_2 forms preferentially when a significant amount of water is present. Based on these observations, we could reverse the selectivity of several reactions by two different methods. Thus, adding a small amount of water during the solvothermal aging of the gels favored the formation of m- ZrO_2 instead of t- ZrO_2 . Conversely, using a stoichiometric amount of O-donor completely prevented the formation of water, as all the oxygen atoms were consumed to form the oxide, and this clearly favored the formation of t- ZrO_2 instead of m- ZrO_2 . The texture of the final ZrO_2 materials does not appear related to the formation of water, but by varying the precursor, the O-donor and the reaction conditions we could obtain practically phase pure ($\geq 95\%$) t- or m- ZrO_2 mesoporous supports with specific surface areas up to $130 \text{ m}^2 \text{ g}^{-1}$ after calcination for 5 h at 500 °C in air.

This study illustrates the richness of NHSG process and the crucial importance of the organic reactions involved. It confirms the interest of NHSG for the synthesis of metal oxide mesoporous supports or catalysts, in the absence of templates and reactivity modifiers. Our next goal will be to apply these routes to the synthesis of t- and m- ZrO_2 supports doped with other oxides for catalytic applications.

Experimental Section

Chemicals

Zirconium(IV) propoxide ($\text{Zr}(\text{OnPr})_4$, 70% in 1-propanol) and zirconium (IV) chloride (ZCL, 99.9%) were purchased from Sigma-Aldrich. Anhydrous benzyl alcohol (BnOH, 99.8%), diisopropylether (DIPE, 99%) and acetophenone (AcPh, 99%) were also purchased from Sigma-Aldrich. Acetic anhydride (Ac_2O , 99%), ethanol (EtOH, 99.5%) and anhydrous acetone (ACE, 99.8%) were purchased from ACROS Organics. 2-pentanone (MPK, 99.5%) was purchased from Alfa Aesar. Zirconium(IV) propoxide ($\text{Zr}(\text{OnPr})_4$, 70% in 1-propanol) was treated before use for 15 h under primary vacuum at 120 °C to remove 1-propanol and obtain pure $\text{Zr}(\text{OnPr})_4$ (ZNP). Complete removal of 1-propanol was checked by FTIR spectrometry, by the absence of the OH stretching band from the alcohol (Figure S1). The water content of all oxygen donors was measured by Karl Fischer titration and, if necessary, they were dried over molecular sieves to ensure adequate drying (<10 ppm H_2O for Ac_2O , DIPE; <20 ppm for ACE, MPK, AcPh; <50 ppm H_2O for EtOH, BnOH). Toluene (Sigma-Aldrich, 99.7%) and dichloromethane (Sigma-Aldrich, 99.8%) were dried over a PureSolve MD5 solvent purification system ($\text{H}_2\text{O} < 10 \text{ ppm}$, controlled with by Karl Fischer titration).

Synthesis of ZrO_2 materials

ZrO_2 samples were prepared from $\text{Zr}(\text{OnPr})_4$ (ZNP) or ZrCl_4 (ZCL) using different O-donors: acetic anhydride (Ac_2O), benzyl alcohol (BnOH), acetophenone (AcPh), 2-pentanone (MPK), acetone (ACE), ethanol (EtOH), or diisopropylether (DIPE). The amounts of precursor, O-donor and solvent (if any), the reaction temperature and reaction time are summarized in Table 1 in main text.

Samples from $\text{Zr}(\text{OnPr})_4$: In a typical synthesis (ZNP-BnOH 200/24), BnOH (10 mL, 96 mmol) was slowly added to 5.3 mmol (1.74 g) of purified $\text{Zr}(\text{OnPr})_4$ (without 1-propanol). After stirring for 5 min, the resulting solution was transferred to a 23 mL stainless steel autoclave (Parr Instruments) with a PTFE lining. To avoid water, these manipulations were carried out in a glovebox under argon atmosphere (<10 ppm of water and O_2). The sealed autoclave was then heated at 200 °C for 24 h in an oven, under autogenous pressure. After reaction, the liquid phase (syneresis liquid) was immediately collected for Karl Fischer and NMR characterization. The gel was thoroughly washed with ether (5 × 30 mL), EtOH (5 × 30 mL) and acetone (5 × 30 mL). Then, it was dried under vacuum (100 Pa) at 120 °C for 5 h. Part of the xerogel was kept for characterization, the rest was calcined in a muffle furnace at 500 °C (heating rate $10^\circ\text{C min}^{-1}$) for 5 h in ambient air. The final oxide was ground into a fine powder for characterization.

To study the influence of water in the solvothermal aging of the gels, two gels were prepared as described above (ZNP- Ac_2O 200/36 and ZNP-ACE 200/12). However, after opening the autoclave, the gels were washed 3 times with dry toluene, then put in an autoclave with 10 mL of toluene containing 2 wt% (20 000 ppm) of water. The autoclaves were then sealed and heated at 200 °C for 36 h (ZNP- Ac_2O 200/36) or 12 h (ZNP-ACE 200/12). After heating, the gels were washed, dried and calcined as described above to give ZNP- Ac_2O 200/36-W200/36 and ZNP-ACE 200/12-W200/12.

Samples from ZrCl_4 : To ensure complete dissolution of ZrCl_4 , high purity ($\geq 99.9\%$) ZrCl_4 was stirred with the O-donor and the solvent (if any) for 30 min. In the case of alcohol O-donors (EtOH, BnOH) the reactants (and solvent, if any) were mixed for 30 min outside the glovebox in a Schlenk tube connected to a Schlenk line under argon to avoid evolution of HCl inside the glovebox. After reaction the gels were washed 3 times with 50 mL CH_2Cl_2 , otherwise the protocol was the same as for the samples prepared from $\text{Zr}(\text{OnPr})_4$.

Characterization

Powder X-ray diffraction (XRD) patterns were collected with a PANalytical X'Pert Pro MPD diffractometer with the $\text{CuK}\alpha$ radiation between 20 and 70° (2θ), with a step of 0.05°. The volume percentage of t- ZrO_2 phase (t-ZrO_2) was calculated from the ratio χ calculated from the areas of the (101) peak of t- ZrO_2 and of the (−111) and (111) peaks of m- ZrO_2 ^[37] according to:

$$\chi = I_t(101) / [I_t(101) + I_m(111) + I_m(-111)]$$

$$\% \text{ t-ZrO}_2 = [1.311\chi / (1 + 0.311\chi)] \times 100\%$$

The areas of the different peaks were measured using the X'Pert HighScore software, by deconvolution of the $\text{K}\alpha 1$ line. The crystallite size was calculated using the same software. Fourier-transform infrared (FTIR) spectra were collected in ATR mode on a Spectrum II PerkinElmer spectrometer. Scanning electron microscopy (SEM) images were obtained with a Hitachi S-4800 electron microscope. High-resolution transmission electron microscopy (TEM) images were obtained using a JEOL 2200FS-200 kV instrument. Nitrogen physisorption isotherms were measured at 77 K with a Micromet-

rics Triflex apparatus; the specific surface area was determined by the BET method, the pore size distribution in the 2 to 100 nm range by the BJH method from the desorption branch. ^1H and ^{13}C NMR spectra in solution were recorded using a Bruker AVANCE 400 MHz spectrometer. The water content in the syneresis liquid was measured on a coulometric Karl Fischer titrator (SI-Analytics TitoLine KF 7500 KF Trace), using the Hydralan Coulomat AK reagent for ketones O-donors and Hydralan Coulomat E reagent for all other O-donors.

Supporting information available

FTIR spectra, N_2 physisorption isotherms, ^1H and ^{13}C NMR spectra of syneresis liquids.

Acknowledgements

Financial support for this work was received from the European Union in the framework of H-CCAT project (NMBP Program Horizon 2020) under grant agreement 720996, and from the French funding agency “Agence Nationale de la Recherche”, project NHYSCAB, grant number ANR-16-CE07-0010. The authors would like to thank Didier Cot (IEM, France) for SEM analyses, and Erwan Oliviero (ICGM) for high resolution TEM analyses.

Conflict of interest

The authors declare no conflict of interest.

Keywords: catalyst support • mesoporous materials • nonhydrolytic sol–gel • sol–gel processes • zirconia

- [1] A. Styskalik, D. Skoda, C. Barnes, J. Pinkas, *Catal.* **2017**, *7*, 168.
- [2] D. P. Debecker, V. Hulea, P. H. Mutin, *Appl. Catal. A* **2013**, *451*, 192–206.
- [3] A. Vioux, *Chem. Mater.* **1997**, *9*, 2292–2299.
- [4] Y.-w. Jun, J.-s. Choi, J. Cheon, *Angew. Chem. Int. Ed.* **2006**, *45*, 3414–3439; *Angew. Chem.* **2006**, *118*, 3492–3517.
- [5] P. H. Mutin, A. Vioux, *Chem. Mater.* **2009**, *21*, 582–596.
- [6] N. Pinna, M. Karmaoui, M.-G. Willinger, *J. Sol-Gel Sci. Technol.* **2011**, *57*, 323–329.
- [7] R. Deshmukh, M. Niederberger, *Chem. Eur. J.* **2017**, *23*, 8542–8570.
- [8] C. J. Cadman, A. Pucci, F. Cellesi, N. Tirelli, *Adv. Funct. Mater.* **2014**, *24*, 993–1003.
- [9] T. Yamaguchi, *Catal. Today* **1994**, *20*, 199–218.
- [10] R. Srinivasan, B. H. Davis in *Materials Synthesis and Characterization* (Ed.: D. L. Perry), Springer Boston, **1997**, pp. 147–188.
- [11] E. I. Kauppi, K. Honkala, A. O. I. Krause, J. M. Kanervo, L. Lefferts, *Top. Catal.* **2016**, *59*, 823–832.
- [12] B. Bachiller-Baeza, I. Rodriguez-Ramos, A. Guerrero-Ruiz, *Langmuir* **1998**, *14*, 3556–3564.
- [13] K. Samson, M. Śliwa, R. P. Socha, K. Góra-Marek, D. Mucha, D. Rutkowska-Zbik, J. F. Paul, M. Ruggiero-Mikołajczyk, R. Grabowski, J. Słoczyński, *ACS Catal.* **2014**, *4*, 3730–3741.
- [14] A. G. Sato, D. P. Volanti, D. M. Meira, S. Damyanova, E. Longo, J. M. C. Bueno, *J. Catal.* **2013**, *307*, 1–17.
- [15] W. Li, H. Huang, H. Li, W. Zhang, H. Liu, *Langmuir* **2008**, *24*, 8358–8366.
- [16] W. Stichert, F. Schüth, S. Kuba, H. Knözinger, *J. Catal.* **2001**, *198*, 277–285.
- [17] R. C. Garvie, M. F. Goss, *J. Mater. Sci.* **1986**, *21*, 1253–1257.
- [18] T. Mitsuhashi, M. Ichihara, U. Tatsuke, *J. Am. Ceram. Soc.* **1974**, *57*, 97–101.
- [19] M. I. Osendi, J. S. Moya, C. J. Serna, J. Soria, *J. Am. Ceram. Soc.* **1985**, *68*, 135–139.
- [20] E. D. Whitney, *Trans. Faraday Soc.* **1965**, *61*, 1991–2000.
- [21] G. Stefanic, S. Musić, *Croat. Chem. Acta* **2003**, *75*, 727–767.
- [22] B. Tyagi, K. Sidhpuria, B. Shaik, R. V. Jasra, *Ind. Eng. Chem. Res.* **2006**, *45*, 8643–8650.
- [23] G. K. Chuah, S. Jaenicke, B. K. Pong, *J. Catal.* **1998**, *175*, 80–92.
- [24] S. Xie, E. Iglesia, A. T. Bell, *Chem. Mater.* **2000**, *12*, 2442–2447.
- [25] M. Jansen, E. Guenther, *Chem. Mater.* **1995**, *7*, 2110–2114.
- [26] C. Warwar Damouny, C. Khoury, O. M. Gazit, *J. Am. Ceram. Soc.* **2019**, *102*, 456–464.
- [27] J. Joo, T. Yu, Y. W. Kim, H. M. Park, F. Wu, J. Z. Zhang, T. Hyeon, *J. Am. Chem. Soc.* **2003**, *125*, 6553–6557.
- [28] Y. Goto, T. Omata, S. Otsuka-Yao-Matsuo, *J. Electrochem. Soc.* **2009**, *156*, K4–K9.
- [29] M. Gateski, V. Petkov, T. Hyeon, J. Joo, M. Niederberger, Y. Ren, *Solid State Commun.* **2006**, *138*, 279–284.
- [30] G. Garnweitner, L. M. Goldenberg, O. V. Sakhno, M. Antonietti, M. Niederberger, J. Stumpe, *Small* **2007**, *3*, 1626–1632.
- [31] T. A. Cheema, G. Garnweitner, *CrystEngComm* **2014**, *16*, 3366–3375.
- [32] P. Stolzenburg, A. Freytag, N. C. Bigall, G. Garnweitner, *CrystEngComm* **2016**, *18*, 8396–8405.
- [33] K. De Keukeleere, J. De Roo, P. Lommens, J. C. Martins, P. Van Der Voort, I. Van Driessche, *Inorg. Chem.* **2015**, *54*, 3469–3476.
- [34] J. Gambe, F. Rémondrière, J. Jouin, L. Portal, P. Thomas, O. Masson, *Inorg. Chem.* **2019**, *58*, 15175–15188.
- [35] F. Tana, M. Messori, D. Contini, A. Cigada, T. Valente, F. Variola, L. De Narodo, F. Bondioli, *Prog. Org. Coat.* **2017**, *103*, 60–68.
- [36] R. Srinivasan, R. J. De Angelis, G. Ice, B. H. Davis, *J. Mater. Res.* **1991**, *6*, 1287–1292.
- [37] H. Toraya, M. Yoshimura, S. Somiya, *J. Am. Ceram. Soc.* **1984**, *67*, C119–C121.
- [38] X. Guo, *Chem. Mater.* **2004**, *16*, 3988–3994.
- [39] P. Arnal, R. J. P. Corriu, D. Leclercq, P. H. Mutin, A. Vioux, *J. Mater. Chem.* **1996**, *6*, 1925–1932.
- [40] A. Aboulaich, B. Boury, P. H. Mutin, *Chem. Mater.* **2010**, *22*, 4519–4521.
- [41] A. M. Escamilla-Pérez, N. Louvain, B. Boury, N. Brun, H. Mutin, *Chem. Eur. J.* **2018**, *24*, 4982–4990.
- [42] Y. Wang, S. Kim, N. Louvain, J. Alauzun, H. Mutin, *Chem. Eur. J.* **2019**, *25*, 4767–4774.
- [43] Y. Wang, J. G. Alauzun, P. H. Mutin, *Chem. Mater.* **2020**, *32*, 2910–2918.
- [44] M. Inoue, H. Kominami, T. Inui, *Appl. Catal. A* **1993**, *97*, L25–L30.
- [45] G. Garnweitner, M. Antonietti, M. Niederberger, *Chem. Commun.* **2005**, 397–399.
- [46] R. Adams, R. W. Hufford, *Org. Synth.* **1922**, *2*, 63.
- [47] G. S. Salvapati, K. V. Ramanamurty, M. Janardanarao, *J. Mol. Catal.* **1989**, *54*, 9–30.
- [48] L. Kubelková, J. Nováková, *Zeolites* **1991**, *11*, 822–826.
- [49] T. Tago, H. Konno, S. Ikeda, S. Yamazaki, W. Ninomiya, Y. Nakasaka, T. Masuda, *Catal. Today* **2011**, *164*, 158–162.
- [50] R. C. Mehrotra, *J. Non-Cryst. Solids* **1988**, *100*, 1–15.
- [51] M. Hu, J. Xu, J. Gao, S. Yang, J. S. P. Wong, R. K. Y. Li, *Dalton Trans.* **2013**, *42*, 9777–9784.
- [52] F. B. F. Silva, E. C. Paris, G. M. da Costa, C. Ribeiro, *RSC Adv.* **2014**, *4*, 53265–53272.
- [53] I. Oliges-Stadler, M. D. Rossell, M. Niederberger, *Small* **2010**, *6*, 960–966.
- [54] A. Braendle, P. Schwendemann, M. Niederberger, W. R. Caseri, *J. Polym. Sci. Part A* **2018**, *56*, 309–318.
- [55] D. P. Debecker, K. Bouchmella, R. Delaigle, P. Eloy, C. Poleunis, P. Bertrand, E. M. Gaigneaux, P. H. Mutin, *Appl. Catal. B* **2010**, *94*, 38–45.
- [56] M. Thommes, K. Kaneko, V. Neimark Alexander, P. Olivier James, F. Rodriguez-Reinoso, J. Rouquerol, S. W. Sing Kenneth, *Pure Appl. Chem.* **2015**, *87*, 1051.

Manuscript received: June 27, 2020

Accepted manuscript online: July 27, 2020

Version of record online: ■■■, 0000

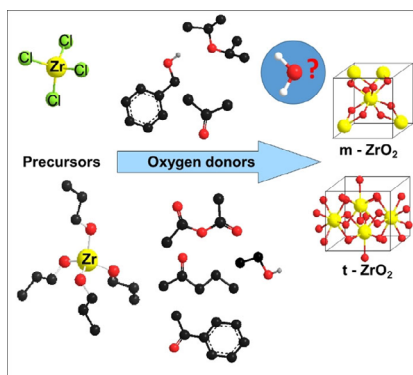
FULL PAPER

Materials Science

 Y. Wang, M. Bouchneb, R. Mighri,
J. G. Alauzun, P. H. Mutin*

■ ■ – ■ ■

  Water Formation in Non-Hydrolytic Sol–Gel Routes: Selective Synthesis of Tetragonal and Monoclinic Mesoporous Zirconia as a Case Study



Water in non-hydrolytic sol-gel: Monitoring *in situ* water formation in non-hydrolytic sol–gel routes to mesoporous zirconia shows that it impacts not only the mechanism of the sol–gel process but also the structure of the final material.